Inorg. Chem. **2008**, *47*, 11620−11632

Targeted Oxidase Reactivity with a New Redox-Active Ligand Incorporating N_2O_2 Donor Atoms. Complexes of Cu(II), Ni(II), Pd(II), Fe(III), and V(V)

Chandan Mukherjee, Thomas Weyhermüller, Eberhard Bothe, and Phalguni Chaudhuri*

Max-Planck-Institute for Bioinorganic Chemistry, Stiftstrasse 34-36, D-45470 Mülheim an der Ruhr, Germany

Received June 25, 2008

The coordination chemistry of the tetradentate ligand *N,N′*-bis(2-hydroxy-3,5-di-*tert*-butylphenyl)-2,2′-diaminobiphenyl H_4L has been studied with the copper(II), nickel(II), palladium(II), iron(III), and vanadium(V) ions. The ligand is non-innocent in the sense that it is readily oxidized in the presence of air to its o-iminobenzosemiquinonato $(L^{\bullet})^{2-}$ radical form. The crystal structures of the diradical compounds, $[Cu^{II}(L^{\bullet})]$ **1**, $[Ni^{II}(L^{\bullet})]$ **2**, $[Pd^{II}(L^{\bullet})]$ **3**, the monoradical high-spin compound $[Fe^{III}(HL^{\bullet})Cl]$ **4**, and the di(μ-methoxo)divanadium(V) compound $[L_2V_2(\mu\text{-}OCH_3)_2]$ **5** without a radical have been determined by X-ray crystallography at 100 K. The biphenyl backbone of the ligand induces a tetrahedral distortion of the metal(II) geometry in **1**, **2**, and **3** having a N_2O_2 coordination environment. The dihedral angles between the metal planes are 35.5° for **1**, 30.8° for **2**, and 22.2° for **3**. Variable-temperature (2−290 K) magnetic susceptibility measurements together with Mössbauer and electron paramagnetic resonance (EPR) spectroscopy establish the electronic structures of the complexes. Electrochemical cyclic voltammetric measurements indicate four one-electron reversible redox processes of the ligand for **1**, **2**, and **3**. Complex **1** is found to catalyze the aerial oxidation of benzylalcohol to benzaldehyde, thus modeling the catalytic function of the copper-containing enzyme Galactose Oxidase (GO). Kinetic measurements in conjunction with EPR and UV−vis spectroscopic studies have been used to decipher the catalytic oxidation process. A ligand-derived redox activity has been proposed as a mechanism in which complex **1** disproportionates in a basic medium to generate the catalytically active species. An "on−off" mechanism of the radicals without apparent participation of the metal center is invoked for the catalytic process, whose intimate mechanism thus differs from that of the enzyme Galactose Oxidase.

Introduction

Our unabated interest in the metal-radical interactions owes its origin to the widespread occurrence of amino acid radicals[1] as electron reservoirs in redox enzymes that activate dioxygen. Such metallobiomolecules have stimulated research to devise structurally defined small molecules[2,3] for elucidation of the molecular basis of their reactivity. Such is the case of Galactose Oxidase (GO),[4] a mononuclear copper enzyme (Type 2 copper, 68 kDa) which uses a modified tyrosyl radical to facilitate the two-electron oxidation of primary alcohols to aldehydes with subsequent reduction of dioxygen to peroxide. The crystal structure[4a,b] of GO shows a distorted square-pyramidal copper site with two histidine nitrogen and two oxygen (from one axial and one equatorial tyrosine) donor atoms, plus an exogenous water in the equatorial site, which is also the binding site for the substrate. The copper(II) center with tyrosine (Tyr 272) radical in the equatorial position which is responsible for hydrogen atom abstraction from the substrate is the active form of Galactose Oxidase. GO thus contains two one-electron redox centers: $1e^-$ per copper, shuttling between Cu(I) and Cu(II), and $1e^-$ from tyrosine radical.

Model studies,[2,3,5] both structural and functional, are continuously providing a profound molecular basis for the

* To whom correspondence should be addressed. E-mail: chaudh@mpi-muelheim.mpg.de.

(1) (a) Holm, R. H.; Solomon, E. I. *Chem. Rev.* **1996**, *96*, 7. (b) Stubbe, J.; van der Donk, W. A. *Chem. Rev.* **1998**, *98*, 705. (c) Chaudhuri, P.; Wieghardt, K. *Prog. Inorg. Chem.* **2001**, *50*, 151. (d) Mahadevan, V.; Klein Gebbink, R. J. M.; Stack, T. D. P. *Curr. Opin. Chem. Biol.* **2000**, *4*, 228. (e) Whittaker, J. W. *Chem. Rev.* **2003**, *103*, 2347. (f) Stubbe, J. *Chem. Commun.* **2003**, 2511. (g) Banerjee, R. *Chem. Rev.* **2003**, *103*, 2081. (h) Holm, R. H.; Solomon, E. I. *Chem. Rev.* **2004**, *104*, 2.

10.1021/ic8011734 CCC: $40.75
Published on Web 11/11/2008

Scheme 1

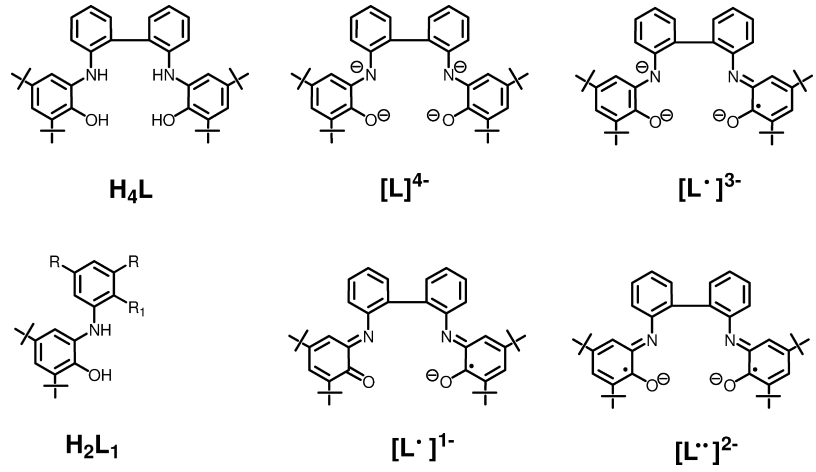

$[Cu^{II}(L^{\bullet\bullet})]$ Complex **1**
$[Ni^{II}(L^{\bullet\bullet})]$ Complex **2**
$[Pd^{II}(L^{\bullet\bullet})]$ Complex **3**
$[Fe^{III}(HL^{\bullet})Cl]$ Complex **4**
$[V^{V}{}_2(\mu_2\text{-}OCH_3)_2(L)_2]$ Complex **5**

active form of the copper-enzyme GO. In the past few years we have been involved in developing bio-inspired catalytic systems based on redox-active "non-innocent" ligands as electron reservoirs;[5,6] such ligand-derived redox activity for transformations of small organic molecules is largely unexplored. Thus, we reported bis(o-iminosemiquinonato)-copper(II) complexes derived from differently substituted *N*-phenyl-2-aminophenol-based ligands H_2L_1 (Scheme 1) as GO-inspired catalytic systems[6d] for oxidation of primary alcohols with aerial oxygen as the sole oxidant to afford aldehydes under mild conditions. These copper(II)-diradical complexes are square-planar within experimental error, thus deviating from the distorted geometry of the copper center in the enzyme GO.[4] To induce distortion toward a tetrahedral coordination and enhance the affinity of the metal center for a fith ligand, we have modified our earlier redox-active ligand system to incorporate the biphenyl backbone[2c] instead of the aniline moiety. Thus, we report here a new "non-innocent" ligand, *N*,*N*′-bis(2-hydroxy-3,5-di-*tert*-butylphenyl)-2,2′-diaminobiphenyl, H_4L, (Scheme 1), which can generate two radical centers, together with its coordinating ability toward transition metals like Cu(II), Ni(II), Pd(II), Fe(III), and V(V) (Scheme 1). Moreover, the copper(II) complex, $[Cu^{II}(L^{\bullet\bullet})]$ **1** has been studied as a catalyst for the aerial oxidation of benzyl alcohol to mimic the function of GO. The newly designed ligand H_4L can thus be conceived as a dimer of H_2L_1 (Scheme 1), our reported earlier ligand.[6−8] Noteworthy in this connection is the report of the anisole-derivative of the ligand in yttrium chemistry.[9]

Experimental Section

Materials and Physical Measurements. Reagent- or analytical-grade materials were obtained from commercial suppliers and used

(2) See for example: (a) Jazddzewski, B. A.; Tolman, W. B. *Coord. Chem. Rev.* **2000**, *633*, 200–202. (b) Michel, F.; Thomas, F.; Hamman, S.; Saint-Aman, E.; Bucher, C.; Pierre, J.-P. *Chem.—Eur. J.* **2004**, *10*, 4115; and references therein. (c) Wang, Y.; Stack, T. D. P. *J. Am. Chem. Soc.* **1996**, *118*, 13097. (d) Itoh, S.; Taki, M.; Fukuzumi, S. *Coord. Chem. Rev.* **2000**, *198*, 3. (e) Sokolowski, A.; Leutbecher, H.; Weyhermüller, T.; Schnepf, R.; Bothe, E.; Bill, E.; Hildebrandt, P.; Wieghardt, K. *J. Biol. Inorg. Chem.* **1997**, *2*, 444. (f) Benisvy, L.; Blake, A. J.; Collison, D.; Davies, E. S.; Garner, C. D.; McInnes, E. J. L.; McMaster, J.; Whittaker, G.; Wilson, C. *Chem. Commun.* **2001**, 1824. (g) Pratt, R. S.; Mirica, L. M.; Stack, T. D. P. *Inorg. Chem.* **2004**, *43*, 8030. (h) Wang, Y.; Dubois, J. L.; Hedman, B.; Hodgson, K. O.; Stack, T. D. P. *Science* **1998**, *279*, 537. (i) Chaudhuri, P.; Hess, M.; Flörke, U.; Wieghardt, K. *Angew. Chem., Int. Ed.* **1998**, *37*, 2217. (j) Chaudhuri, P.; Hess, M.; Weyhermüller, T.; Wieghardt, K. *Angew. Chem., Int. Ed.* **1999**, *38*, 1095.

(3) (a) Chaudhuri, P.; Hess, M.; Müller, J.; Hildenbrand, K.; Bill, E.; Weyhermüller, T.; Wieghardt, K. *J. Am. Chem. Soc.* **1999**, *121*, 9599. (b) Thomas, F.; Gellon, G.; Gautier-Luneau, I.; Saint-Aman, E.; Pierre, J.-L. *Angew. Chem., Int. Ed.* **2002**, *41*, 3047. (c) Paine, T. K.; Weyhermüller, T.; Wieghardt, K.; Chaudhuri, P. *Dalton Trans.* **2004**, 2092.

(4) (a) Ito, N.; Phillips, S. E. V.; Stevens, C.; Ogel, Z. B.; McPherson, M. J.; Keen, J. N.; Yadav, K. D. S.; Knowles, P. F. *Nature* **1991**, *350*, 87. (b) Ito, N.; Phillips, S. E. V.; Yadav, K. D. S.; Knowles, P. F. *J. Mol. Biol.* **1994**, *238*, 799. (c) Wachter, R. M.; Branchaud, B. P. *J. Am. Chem. Soc.* **1996**, *118*, 2782. (d) Whittaker, J. W.; Whittaker, M. M. *Pure Appl. Chem.* **1998**, *70*, 903. (e) Wright, C.; Sykes, A. G. *J. Inorg. Biochem.* **2001**, *85*, 237.

(5) Chaudhuri, P.; Wieghardt, K.; Weyhermüller, T.; Paine, T. K.; Mukherjee, S.; Mukherjee, C. *Biol. Chem* **2005**, *386*, 1023.

(6) (a) Mukherjee, S.; Weyhermüller, T.; Bothe, E.; Wieghardt, K.; Chaudhuri, P. *Dalton Trans.* **2004**, 3842. (b) Mukherjee, C.; Weyhermüller, T.; Bothe, E.; Chaudhuri, P. *C. R. Chim.* **2007**, *10*, 313. (c) Mukherjee, C.; Weyhermüller, T.; Bothe, E.; Rentschler, E.; Chaudhuri, P. *Inorg. Chem.* **2007**, *46*, 9895. (d) Mukherjee, C.; Pieper, U.; Bothe, E.; Bachler, V.; Bill, E. Weyhermüller, T.; Chaudhuri, P. *Inorg. Chem.* **2008**, *47*, 8943. (e) Chaudhuri, P.; Bill, E.; Wagner, R.; Pieper, U.; Biswas, B.; Weyhermüller, T. *Inorg. Chem.* **2008**, *47*, 5549.

(7) See for example: (a) Verani, C. N.; Gallert, S.; Bill, E.; Weyhermüller, T.; Wieghardt, K.; Chaudhuri, P. *Chem. Commun.* **1999**, 1747. (b) Chun, H.; Chaudhuri, P.; Weyhermüller, T.; Wieghardt, K. *Inorg. Chem.* **2002**, *41*, 790. (c) Mukherjee, S.; Weyhermüller, T.; Wieghardt, K.; Chaudhuri, P. *Dalton Trans.* **2003**, 3483. (d) Mukherjee, S.; Weyhermüller, T.; Bothe, E.; Wieghardt, K.; Chaudhuri, P. *Dalton Trans.* **2004**, 3842. (e) Kokatam, S.; Weyhermüller, T.; Bothe, E.; Chaudhuri, P.; Wieghardt, K. *Inorg. Chem.* **2005**, *44*, 3709. (f) Mukherjee, S.; Weyhermüller, T.; Bill, E.; Wieghardt, K.; Chaudhuri, P. *Inorg. Chem.* **2005**, *44*, 7099. (g) Chaudhuri, P.; Wagner, R.; Pieper, U.; Biswas, B.; Weyhermüller, T. *Dalton Trans.* **2008**, 1286.

(8) Kokatam, S.; Weyhermüller, T.; Bothe, E.; Chaudhuri, P.; Wieghardt, K. *Inorg. Chem.* **2005**, *44*, 3709.

(9) O'Shaughnessy, P. N.; Gillespie, K. M.; Knight, P. D.; Munslow, I. J.; Scott, P. *Dalton Trans.* **2004**, 2251.

without further purification, except those for electrochemical measurements. Elemental analyses (C, H, N, and metal) were performed by the Microanalytical Laboratory, Mülheim, Germany. Fourier-transform IR spectra of the samples in KBr disks were recorded with a Perkin-Elmer 2000 FT-IR instrument. Electronic absorption spectra in solution were measured with a Perkin-Elmer Lambda 19 spectrophotometer. Magnetic susceptibilities of powdered samples were recorded with a superconducting quantum interference device (SQUID) magnetometer in the temperature range 2−290 K with an applied field of 1 T. Experimental susceptibility data were corrected for the underlying diamagnetism using Pascal's constants and for the temperature-independent paramagnetism contributions. Mass spectra were recorded with either a Finnigan MAT 8200 (electron ionization, EIMS) or a MAT 95 (electrospray, ESI-MS) instrument. A Bruker DRX 400 instrument was used for NMR spectroscopy. X-band electron paramagnetic resonance (EPR) spectra were recorded with a Bruker ELEXSYS E500 spectrometer equipped with a helium flow cryostat (Oxford Instruments ESR 910). Cyclic voltammograms (CV) were recorded using a conventional three-electrode arrangement, consisting of a glassy-carbon working electrode (of 2 mm diameter), an Ag/Ag^+ (0.01 M $AgNO_3$) reference electrode, and a Pt-wire counter electrode. Small amounts of ferrocene were added as an internal standard after completion of an experiment, and potentials are referenced versus the ferrocenium/ferrocene (Fc^+/Fc) couple. Potential control was achieved using an EG&G potentiostat/-galvanostat (model 273A) with M270 software, and solutions of the complexes in CH_2Cl_2 containing 0.1 M $[(n\text{-}Bu)_4N]PF_6$ as supporting electrolyte were employed throughout.

Controlled-potential electrolysis at an appropriate fixed potential was performed at −25 °C in a jacketed quartz cell with the same type of reference electrode, a Pt-mesh working electrode, and a Pt-brush counter electrode. The cell (optical path length 0.5 cm) was mounted directly in a spectrophotometer (Hewlett-Packard HP 8453), allowing us to record UV−vis spectra in situ during electrolysis. After the completion of electrolysis, samples of the electrolyzed solutions were taken and rapidly frozen by liquid nitrogen for EPR analysis.

Preparation of the Ligand *N*,*N*′-bis(2-hydroxy-3,5-ditert-butylphenyl)-2,2′-diaminobiphenyl, H_4L. As the reduction of aryl nitro groups by the palladium−sodium borohydride system might produce a multiplicity of products,[10] we have used a modified procedure for the hydrogenation. To dry methanol (130 mL) were added 2,2′-dinitrobiphenyl (6.1 g; 25 mmol) followed by charcoal/Pd catalyst (0.9 g) with stirring under argon. After 5 min stirring, ammonium formate (14.5 g; 230 mmol) was added, and the stirring was continued for 45 min, during which time the evolution of gas subsided. The reaction mixture was filtered through Celite to make it free from the catalyst. The light-yellow filtrate was concentrated on a rotary evaporator to yield a light yellow solid. The solid after dissolving in diethylether (100 mL) was treated with water (40 mL). The product 2,2′-diaminobiphenyl was extracted twice (2 × 100 mL) into ether from the aqueous layer, and the ethereal extract was dried over Na_2SO_4. A yellow-white solid (4.49 g) was isolated after evaporation of ether. Yield: 93%, EI-MS: *m*/*z* 184 $[M^+]$.

To a solution of 3,5-di-*tert*-butylcatechol (10.2 g; 46 mmol) and triethylamine (0.3 mL) in *n*-hexane (150 mL) was added solid 2,2′-diaminobiphenyl (4.56 g; ∼23 mmol). The resulting solution was stirred in air for 20 h, after which time a white (brownish) solid was collected by filtration, washed with *n*-hexane, and air-dried. The yield was 6.69 g (49%) based on the starting catechol. The purity of the ligand was checked by gas chromatography. Purity = 98%. Mp: 198−199 °C. EI-MS: *m*/*z* 592 (100%) $[M]^+$, 536 (11.8%) $[M - C_4H_9]^+$, 372 (16.7%) $[M - C_{14}H_{16}O]^+$. ^1H NMR (400 MHz, $CDCl_3$): δ 1.22 (s, 18H), 1.39 (s, 18H), 5.08 (s, 2H), 6.30 (br, 2H), 6.59−6.61 (d, 2H), 6.94−6.98 (m, 4H), 7.18−7.30 (m, 6H). IR(KBr, cm^{-1}): 3479s, 3371s, 2957−2868s, 1595s, 1579s, 1509s, 1476s, 1450s, 1426s, 1363s, 1317s, 1220s, 1201s, 1156m, 1120m, 1005m, 976m, 880s, 823m, 804m, 754s. Anal. Calcd for $C_{40}H_{52}N_2O_2$ (592.8): C, 81.04; H, 8.84; N, 4.73. Found: C, 80.6; H, 9.1; N, 4.8. Single crystals suitable for X-ray diffraction were grown from CH_2Cl_2/CH_3CN under argon.

Preparation of Complexes. Complex 1 $[Cu^{II}(L^{\bullet})]$. To a solution of the ligand, H_4L (1.185 g; 2 mmol), Et_3N (0.1 mL) in dry acetonitrile under argon (30 mL) was added solid $[Cu^I(CH_3CN)_4]ClO_4$ (0.655 g; 2 mmol). The solution was stirred under argon for 0.5 h and then in the presence of air for 1 h. The solution was allowed to be concentrated by a gentle Ar-stream to yield a dark crystalline solid of **1**, which was collected by filtration. Yield: 0.98 g (∼75%). Single crystals suitable for X-ray diffraction were grown from a CH_2Cl_2/CH_3CN solvent mixture (1:1). Anal. Calcd for $C_{40}H_{48}CuN_2O_2$: C, 73.64; H, 7.42; N, 4.29; Cu, 9.74. Found: C, 73.1; H, 7.5; N, 4.3; Cu, 9.8. ESI (positive)-MS in CH_2Cl_2: *m*/*z* 651.6 (100%) $[M^+]$. IR(KBr, cm^{-1}): 2959−2866, 1580, 1515, 1462, 1421, 1384, 1366, 1329, 1266, 1202, 1175, 1109, 1026, 993, 912, 868, 856, 778, 765, 747, 722, 646.

Complexes 2, $[Ni^{II}(L^{\bullet})]$ and 3 $[Pd^{II}(L^{\bullet})]$. A solution of the ligand (1.185 g; 2 mmol), triethylamine (0.2 mL) and either $NiCl_2 \cdot 6H_2O$ (0.475 g; 2 mmol) or $PdCl_2$ (0.345 g; 2 mmol) in acetonitrile (30 mL) was stirred at room temperature in the presence of air for 1 h. A dark brown precipitate formed which was collected by filtration, washed with acetonitrile, and air-dried. X-ray quality crystals were obtained by crystallization from a CH_3CN/CH_2Cl_2 mixture (1:1).

$[Ni^{II}(L^{\bullet})]$ (2). Yield: 0.96 g (∼70%). Anal. Calcd for $C_{40}H_{48}NiN_2O_2$: C, 74.220; H, 7.47; N, 4.33; Ni, 9.06. Found: C, 73.3; H, 7.4; N, 4.2; Ni, 8.6. ESI (positive)-MS in CH_2Cl_2: *m*/*z* 646.4 (100%) $[M^+]$. EI-MS: *m*/*z* 646 (100%), 647 (59.5%), 648 (54.9%), 649 (27.7%), 650 (13.0%). IR(KBr, cm^{-1}): 2958, 2904, 2865, 1534, 1521, 1474, 1459, 1421, 1383, 1363, 1314, 1286, 1261, 1228, 1199, 1174, 1128, 1109, 1028, 998, 916, 869, 857, 765, 775, 748, 730, 669, 646. ^1H NMR (CD_2Cl_2, 400 MHz, 300 K): δ = 1.14 (s, 9H), 1.27 (s, 9H), 1.53 (s, 9H), 1.56 (s, 9H), 6.75 (d, 2H), 7.22 (d, 2H), 7.26 (d, 2H), 7.30 (t, 2H), 7.336−7.40 (m, 2H), 7.53−7.55 (d, 2H). UV−vis in CCH_2Cl_2: λ, nm (ε, M^{-1} cm^{-1}); 981(13670), 746(1950), 505(1630), 336(6410).

$[Pd^{II}(L^{\bullet})]$ (3). Yield: 1.05 g (∼75%). Anal. Calcd for $C_{40}H_{48}PdN_2O_2$: C, 69.10; H, 6.96; N, 4.03; Pd, 15.31. Found: C, 68.8; H, 7.2; N, 4.0; Pd, 14.9. ESI (positive)-MS in CH_2CN: *m*/*z* 694.35 $[M^+]$. EI-MS: *m*/*z* 692 (30%), 693 (70%), 694(100%), 695(50%), 696(80%), 697(40%), 698(40%), 699(20%). IR(KBr, cm^{-1}): 2958, 2904, 2865, 1581, 1519, 1471, 1429, 1404, 1384, 1364, 1309, 1283, 1256, 1226, 1197, 1172, 1127, 1111, 1028, 997, 918, 871, 856, 825, 775, 764, 748, 660, 607. ^1H NMR (CD_2Cl_2, 400 MHz, 300 K): δ 1.19 (s, 9H), 1.26 (s, 9H), 1.55 (s, 9H), 1.60 (s, 9H), 6.80 (s, 2H), 7.0 (br, 2H), 7.26−7.36 (m, 4H), 7.49−7.51 (d, 2H), 7.61 (d, 2H). UV−vis in CH_2Cl_2: λ, nm (ε, M^{-1} cm^{-1}), 961(26600), 756(6170), 554(3100), 475(4360), 345(14665).

Complex 4, $[Fe^{III}(HL^{\bullet})Cl]$. A solution of the ligand H_4L (0.592 g; 1 mmol), triethylamine (0.1 mL), and anhydrous $FeCl_3$ (0.33 g; 1 mmol) in acetonitrile (30 mL) was stirred at ambient temperature in the presence of air for 1 h. The separated dark greenish-blue microcrystalline solid was collected by filtration and washed with acetonitrile. Single crystals for the X-ray diffractometry were

(10) (a) Smith, W. B. *Heterocycl. Chem.* **1987**, *24*, 745. (b) Buntrock, B. E.; Taylor, E. C. *Chem. Rev.* **1968**, *68*, 209.

obtained by slow evaporation from a $CH_2Cl_2-CH_3CN$ (1:1) solvent mixture. Yield: 0.520 g (~75%). Anal. Calcd for $C_{40}H_{49}N_2O_2ClFe$: C, 70.53; H, 7.25; N, 4.11; Cl, 5.21; Fe, 8.20. Found: C, 70.8; H, 7.2; N, 4.1; Fe, 8.2. ESI (positive)-MS in CH_2Cl_2: *m/z* 644.4 (100%) $[M - H^{\bullet} - Cl]^+$. ESI (negative)-MS in CH_2Cl_2: *m/z* 679.5 (100%) [M − H]. IR(KBr, cm^{-1}): 3280, 2956, 2867, 2904, 1586, 1525, 1497, 1477, 1411, 1387, 1359, 1302, 1256, 1203, 1179, 1115, 1029, 993, 974, 927, 913, 886, 870, 830, 798, 779, 764, 752, 734, 666, 595, 488. UV−vis in CH_2Cl_2: λ, nm (ε, M^{-1} cm^{-1}), 707(11100), 443(11300).

Complex 5, $[V^{V}(\mu_2\text{-}OCH_3)_2(L)_2]$. Under an argon atmosphere solid $VOSO_4 \cdot 5H_2O$ (0.51 g; 2 mmol) was added to a solution of the ligand H_4L (1.05 g; 2 mmol) in methanol. Addition of triethylamine (0.2 mL) changed the solution to deep blue which was stirred under argon for an hour and then the stirring was continued in the presence of air for further 2 h. The solution kept at room temperature afforded crystalline dark-blue solid which was collected by filtration. Yield: 0.47 g (35%). X-ray quality crystals were grown from a dichloromethane solution. Anal. Calcd for $C_{82}H_{102}N_4O_6V_2$: C, 73.41; H, 7.66; N, 4.18; V, 7.59. Found: C, 73.1; H, 7.6; N, 4.2; V, 7.8. ESI (possitive)-MS in CH_2Cl_2: *m/z* 1340.5 (100%) $[M]^+$, 1295.5 (~28%) $[M - C_3H_9]^+$, 1230.6 (60%) $[M - 2 \times C_4H_9]^+$. ESI (negative)-MS in CH_2Cl_2: *m/z* 1340.6 (~10%) $[M]^-$, 1230.7 (~30%) $[M - 2 \times C_4H_9]^-$, 655.4 (100%) $[M/_2 - CH_3]$. EI-MS: *m/z* 670(100%)$[M/_2]^+$. IR(KBr, cm^{-1}): 3061w, 2952, 2903, 2866, 1577, 1543, 1474, 1428, 1392, 1361, 1312, 1254, 1229, 1200, 1164, 1028, 1000, 915, 864, 853, 839, 764, 683, 650, 608, 551, 520.

X-ray Crystallographic Data Collection and Refinement of the Structures. A colorless single crystal of **H_4L** and dark crystals of complexes **1**−**5** were coated with perfluoropolyether, picked up with nylon loops, and mounted in the nitrogen cold stream of the diffractometer at 100 K. A Bruker-Nonius KappaCCD diffractometer equipped with a Mo-target rotating-anode X-ray source and graphite monochromated Mo−Kα radiation (λ = 0.71073Å) was used throughout. Final cell constants were obtained from least-squares fits of all measured reflections.

Intensity data of **H_4L** were corrected for absorption using intensities of redundant reflections. The data set of **3** was corrected for absorption using the Gaussian method embedded in XPREP.[11a] The structures of metal containing compounds were readily solved by Patterson methods and subsequent difference Fourier techniques. The structure of **H_4L** was solved with direct methods. The Siemens ShelXTL[11a] software package was used for solution and artwork of the structures, and ShelXL97[11b] was used for the refinement. All non-hydrogen atoms were anisotropically refined, and hydrogen atoms attached to carbon were placed at calculated positions and refined as riding atoms with isotropic displacement parameters. Acidic hydrogen atoms in compound **H_4L**, namely H(h) and H(1), were located from the difference map and isotropically refined with restrained bond distances and displacement parameters.

A *t*-butyl group in **3** was found to be disordered by rotation. A split atom model with an occupation ratio of about 0.79:0.21 and restrained bond distances and anisotropic displacement parameters was refined using EADP and SADI instructions of ShelXL97.[11b] One of the two crystallographically independent complex molecules in **5** also showed such disorder of a *t*-butyl group. A ratio of about 0.77:0.23 was refined here, using restraints as explained above. Additionally, a CH_2Cl_2 solvent molecule in **5** is disordered. Two split positions with restrained C−Cl and Cl−Cl distances and equal anisotropic displacement parameters for corresponding atoms was refined giving an occupation ratio of about 0.84:016. Crystallographic data of the compounds are listed in Table 1.

Procedure for the Aerial Oxidation of Benzylalcohol and Determination of the Concentration of Benzaldehyde. A solution of 2.5×10^{-4} M of **1**, benzylalcohol in the range of 10×10^{-4}−2.5×10^{-2} M and 0.9 equiv (related to benzylalcohol) of $^{n}Bu_4NOMe$ in 20 mL of CH_2Cl_2 was stirred in air for the oxidation. The solution was diluted as required for acquisition of the electronic spectra using a blank with the catalyst. The concentration of benzaldehyde was calculated on the basis of its molar extinction coefficient (ε_{290} = 1.22×10^3 M^{-1} cm^{-1}) at 290 nm. Benzaldehyde was quantitatively also determined by liquid chromatography (LC) measurements using a column, Nucl.-5-C/8 Sel-214, UV = 250 nm, gas = MeOH/H_2O (1:1 v/v).

Results and Discussion

The ligand H_4L is readily available in a good yield from the reaction of 2,2′-diaminobiphenyl and 3,5-di-*tert*-butylcatechol in the presence of air and the base triethylamine. The reactions of the ligand with different metal salts such as $[Cu^{I}(CH_3CN)_4]ClO_4$, $NiCl_2 \cdot 6H_2O$, $PdCl_2$, $FeCl_3$ or $VOSO_4 \cdot 5H_2O$ in CH_3CN or CH_3OH in the presence of air affords dark crystalline materials **1**−**5**, respectively. They are completely air-stable in the solid state and also in solution for a few days.

The IR spectra of **1**−**3** are very similar and do not warrant any special discussion; the bands are listed in the Experimental Section. Noteworthy is the absence of the bands at 3479 and 3371 cm^{-1}, attributable to ν(OH) and ν(NH) vibrations, respectively, of the ligand, in complexes **1**−**3**, indicating the absence of these protons in the coordinated ligands. A noticeable feature in the IR spectrum of **4** is the presence of a strong sharp band at 3280 cm^{-1}, indicating the presence of the -NH group in **4**. Moreover, the strong bands at 1477 and 1265 cm^{-1}, attributable to ν(C−O$^{\bullet}$) and phenolic ν(C−O), indicate that the ligand is present in the mixed-valent iminosemiquinone-aminophenolate form in complex **4**. Complex **5** does not exhibit any sharp band in the 900−1000 cm^{-1} region, which is in accord with the absence of the V=O structural unit in the complex.

Complexes **2**, **3**, and **5** are diamagnetic as is evidenced by SQUID measurements in the temperature range 2−290 K. The diamagnetic nature of **5** was further confirmed by measuring its ^{51}V NMR spectrum in CH_2Cl_2 at room temperature; a broad peak at $\delta \sim 120$ ppm (relative to $VOCl_3$) corroborates the assignment of a formal oxidation state of +V (see X-ray structure) for the vanadium ion with a d^0 electron configuration. Details of the ^1H NMR spectra for **2** and **3** are given in the Experimental Section and are in line with their diamagnetism.

EI and ESI mass spectrometric measurements have been proven to be very useful tools for characterizing all complexes (Experimental Section), which show the molecule-ion peak in most of the cases as the base peak (100%). Thus, the mass spectra of the complexes confirm the compositions $[MC_{40}H_{48}N_2O_2]$ (M = Cu, Ni, Pd) for **1**, **2**, and **3**, $[FeC_{40}H_{49}N_2O_2Cl]$ for **4**, and $[VC_{41}H_{51}N_2O_3]_2$ for **5**.

Description of the Structures. To gain insight into the metrical parameters of the ligand, H_4L, we have determined the structure of the uncoordinated ligand by X-ray diffrac-

Table 1. Crystallographic Data and Structure Refinement Parameters for H_4L, **1**, **2**, **3**, **4** and **5**·1.25CH_2Cl_2

	H_4L	**1**	**2**
empirical formula	$C_{40}H_{52}N_2O_2$	$C_{40}H_{48}CuN_2O_2$	$C_{40}H_{48}N_2NiO_2$
fw	592.84	652.34	647.51
temperature (K)	100(2)	100(2)	100(2)
wavelength (Å)	1.54178	0.71073	0.71073
crystal system, space group	monoclinic, *C*2/*c*, No. 15	monoclinic, $P2_1/n$, No. 14	monoclinic, $P2_1/n$, No. 14
unit cell dimensions	a = 31.858(2) Å	a = 9.4200(6) Å	a = 9.4934(3) Å
	b = 9.8004(5) Å	b = 18.5916(14) Å	b = 18.4206(6) Å
	c = 11.4541(6) Å	c = 19.784(2) Å	c = 19.70227(8) Å
	β = 101.833(3)°	β = 101.55(1)°	β = 101.49(1)°
volume (Å^3), Z	3500.2(3), 4	3394.7(5), 4	3376.4(2), 4
calcd density (Mg/m^3)	1.125	1.276	1.274
abs. coeff. (mm^{-1})	0.524	0.680	0.612
F(000)	1288	1388	1384
crystal size (mm)	0.34 × 0.17 × 0.60	0.18 × 0.06 × 0.06	0.12 × 0.06 × 0.06
θ range for data collection (deg)	2.83 to 64.98	3.42 to 26.00	3.42 to 27.50
reflns. collected/unique	37811/2949 [R(int) = 0.0724]	45253/6630 [R(int) = 0.1060]	53654/7708 [R(int) = 0.1047]
abs. correction	semiempirical from equiv.	not corrected	not corrected
refinement method	full-matrix least-squares on F^2	full-matrix least-squares on F^2	full-matrix least-squares on F^2
data/restraints/parameters	2949/2/211	66330/0/406	7708/0/406
GOF on F^2	1.107	1.039	1.029
final R indices [$I > 2\sigma(I)$]	R1 = 0.0515, wR2 = 0.1259	R1 = 0.0580, wR2 = 0.1244	R1 = 0.0462, wR2 = 0.0910
R indices (all data)	R1 = 0.0633, wR2 = 0.1362	R1 = 0.0936, wR2 = 0.1409	R1 = 0.0659, wR2 = 0.0986
largest diff. peak and hole (e/Å^3)	0.363 and −0.249	0.849 and −0.687	0.338 and −0.472

	3	**4**	**5**·1.25CH_2Cl_2
empirical formula	$C_{40}H_{48}N_2O_2Pd$	$C_{40}H_{49}ClFeN_2O_2$	$C_{83.25}H_{104.5}Cl_{2.50}N_4O_6V_2$
fw	695.20	681.11	1447.71
temperature (K)	100(2)	100(2)	100(2)
wavelength (Å)	0.71073	0.71073	0.71073
crystal system, space group	monoclinic, $P2_1/n$, No. 14	triclinic, $P\bar{1}$, No. 2	monoclinic, $P2_1/n$, No. 14
unit cell dimensions	a = 9.5172(6) Å	a = 9.1566(5) Å	a = 23.6897(6) Å
	b = 18.5949(12) Å	b = 10.1701(5) Å	b = 24.5174(7) Å
	c = 20.290(2) Å	c = 19.7866(8) Å	c = 27.9324(9) Å
	β = 100.88(1)°	α = 94.374(5)°, β = 96.805(5)°, γ = 91.558(5)°	β = 104.534(6)°
volume (Å^3), Z	3526.2(5), 4	1823.07(15), 2	15704.2(8), 8
calcd density (Mg/m^3)	1.310	1.241	1.225
abs. coeff. (mm^{-1})	0.562	0.523	0.377
F(000)	1456	724	6148
crystal size (mm)	0.14 × 0.02 × 0.02	0.14 × 0.06 × 0.03	0.14 × 0.04 × 0.02
θ range for data collection (deg)	3.00 to 23.35	2.96 to 27.50	2.91 to 22.50
reflns. collected/unique	20043/5081 [R(int)=0.0889]	29940/8345 [R(int)=0.0786]	114758/20469 [R(int)=0.0777]
abs. correction	Gaussian, face-indexed	none	none
refinement method	full-matrix least-squares fit on F^2	full-matrix least-squares fit on F^2	full-matrix least-squares fit on F^2
data/restraints/parameters	5081/31/419	8345/0/430	20469/64/1798
GOF on F^2	1.018	1.070	1.048
final R indices [$I > 2\sigma(I)$]	R1 = 0.0461, wR2 = 0.0829	R1 = 0.0617, wR2 = 0.1196	R1 = 0.0603, wR2 = 0.1359
R indices (all data)	R1 = 0.0813, wR2 = 0.0943	R1 = 0.0930, wR2 = 0.1324	R1 = 0.0886, wR2 = 0.1512
largest diff. peak and hole (e/Å^3)	0.448 and −0.412	0.513 and −0.584	0.886 and −0.936

tometry. X-ray quality crystals of H_4L were grown from dichloromethane. The structure of the ligand H_4L in the solid state is shown in Figure 1. The structure of the ligand H_4L serves as benchmark for the geometrical details for the fully reduced (i.e., aromatic) form. The six C−C bond distances

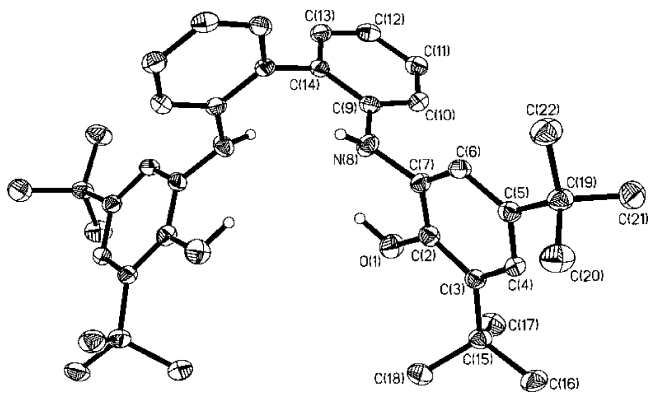

Figure 1. Perspective view of H_4L.

in the o-aminophenol part are observed in the narrow range 1.387(3)−1.405(3) Å (average 1.394 Å), indicating the presence of six nearly equidistant aromatic C−C bonds. Similarly, the biphenyl part exhibits C−C bond distances also of nearly equal length at average 1.391 Å (range 1.382(3)−1.407(3) Å). The C(7)−N(8) and C(9)−N(8) bond distances at 1.432(3) and 1.404(3) Å, respectively, are typical of C−N single bonds, and the C(2)−O(1) distance at 1.376(2) Å is typical for aromatic phenols. Supporting Information, Table S1 lists the selected bond distances and angles for the ligand H_4L.

The crystal structures of complexes **1**−**5** have been determined by single-crystal X-ray crystallography at 100(2) K. The molecular structure of **1**, [$Cu^{II}(L^{\bullet\bullet})$], is shown in Figure 2. The geometry around the Cu(1) center is distorted square-planar N_2O_2, with two nitrogen donor atoms N(8) and N(21) of the ligand $[L^{\bullet\bullet}]^{2-}$ necessarily in the cis positions with respect to each other (as are the two oxygen atoms,

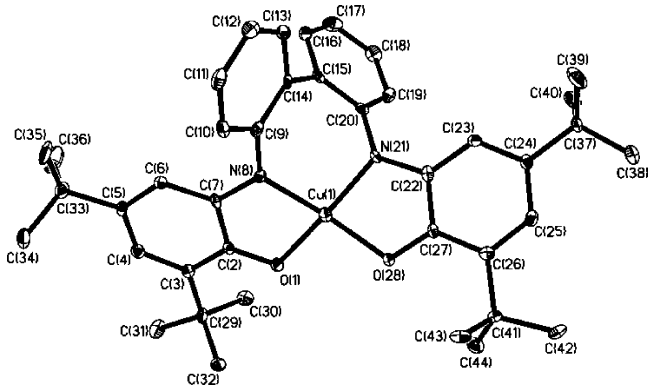

Figure 2. Molecular structure of complex **1**, $[Cu^{II}(L^{\bullet})]$.

O(1) and O(28)). The C−C bond distances for the biphenyl ring in complex **1** have been found to lie within the range of 1.395 ± 0.018 Å, indicating that these C−C lengths are equidistant and the conjugation in the phenyl rings is retained. As expected the C(14)−C(15) bond is much longer at 1.491(5) Å and has single bond character. In contrast, the six C−C distances in the *tert*-butyl-substituted rings with C(2) to C(7) or with C(22) to C(27) are not equidistant: the typical pattern of the iminobenzosemiquinone radicals[7] of a short, a long, and again a short, and three adjacent long bonds are found. For example: C(3)−C(4) 1.377(5), C(4)−C(5) 1.434(5), C(5)−C(6) 1.368(5), C(6)−C(7) 1.417(5), C(7)−C(2) 1.452(5), C(2)−C(3) 1.436(5) Å. Thus, the rings with the *tert*-butyl groups adopt a quinoid-type structure. The coordination geometry around the nitrogen donors, N(8) and N(21), is planar indicating that these nitrogens are three-coordinate (sp^2 hybridization) and not protonated. Additionally, the bond lengths C(7)−N(8) and C(22)−N(21) at 1.342(4) and 1.356(4) Å, respectively, and C(2)−O(1) and C(27)−O(28) at 1.295(4) and 1.304(4) Å, respectively, are significantly shorter than the corresponding C−N and C−O bonds of order one. The geometrical parameters for **1** are identical within experimental error to those for the iminobenzosemiquinonate radical ligands reported for other similar complexes in the literature.[7,8,12]

Consequently, the metal atom Cu(1) can safely be assigned to the physical oxidation state +II. Table 2 lists the selected bond distances and angles for **1**.

The structures of the neutral complexes in crystals of **2** and **3** are very similar to that in **1**; hence, the structures are not shown and are displayed in Supporting Information, Figures S1 and S2. Supporting Information, Tables S2 and S3 give selected bond distances and angles for both complexes. According to structural analyses both **2** and **3** are formulated as bis(radical)-metal(II), $[M^{II}(L^{\bullet})]$ complexes [M = Ni(II) **2**, Pd(II) **3**] and are in accord with their diamagnetic nature because of strong antiferromagnetic interactions between the radicals. To quantify the distortion of the metal geometry from ideal square-planar coordination, the dihedral angle between the planes comprising Cu(1)-N(8)C(7)C(2)O(1) and Cu(1)N(21)C(22)C(27)O(28) atoms (Figure 2) in complex **1**, together with the corresponding angles for **2** (Ni) and **3** (Pd), were evaluated to be 35.5°, 30.8°, and 22.2° for **1**, **2**, and **3**, respectively. Thus, a significant distortion toward a tetrahedral coordination, even for a second-row transition metal ion like Pd(II), is observed in accordance with our expectation for the new non-innocent ligand H_4L bearing a biphenyl backbone. It is to be noted that such tetrahedral distortion of square planar geometry is known in palladium chemistry,[13] in which the almost planar ligands alleviate their mutual steric interaction through a *twist* conformation.

Table 2. Selected Bond Distances (Å) and Angles (deg) for Complex **1**, $[Cu^{II}(L^{\bullet})]$

Cu(1)−N(8)	1.925(3)	C(4)−C(5)	1.434(5)
Cu(1)−N(21)	1.919(3)	C(5)−C(6)	1.368(5)
Cu(1)−O(1)	1.925(2)	C(6)−C(7)	1.417(5)
Cu(1)−O(28)	1.925(2)	C(22)−N(21)	1.356(5)
C(2)−O(1)	1.295(4)	C(22)−C(23)	1.418(5)
C(7)−N(8)	1.342(4)	C(23)−C(24)	1.373(5)
C(2)−C(7)	1.452(5)	C(24)−C(25)	1.420(5)
C(2)−C(3)	1.436(5)	C(25)−C(26)	1.386(5)
C(3)−C(4)	1.377(5)	C(26)−C(27)	1.429(5)
C(9)−N(8)	1.405(5)	C(27)−O(28)	1.304(5)
C(9)−C(10)	1.403(5)	C(20)−C(15)	1.410(5)
C(10)−C(11)	1.413(5)	C(15)−C(16)	1.406(5)
C(11)−C(12)	1.392(5)	C(16)−C(17)	1.380(5)
C(12)−C(13)	1.376(5)	C(17)−C(18)	1.382(5)
C(13)−C(14)	1.403(5)	C(18)−C(19)	1.392(5)
C(14)−C(9)	1.413(5)	C(19)−C(20)	1.406(5)
O(1)−Cu(1)−N(8)	84.49(11)	O(1)−Cu(1)−O(28)	99.72(10)
N(8)−Cu(1)−N(21)	100.23(12)	O(1)−Cu(1)−N(21)	155.12(10)
N(21)−Cu(1)−O(28)	85.3(11)	O(28)−Cu(1)−N(8)	157.41(11)
C(27)−O(28)−Cu(1)	111.2(2)	C(2)−O(1)−Cu(1)	111.5(2)
C(22)−N(21)−C(20)	123.2(3)	C(7)−N(8)−C(9)	122.8(3)
Cu(1)−N(21)−C(20)	121.8(3)	C(9)−N(8)−Cu(1)	124.5(3)
C(22)−N(21)−Cu(1)	111.6(3)	C(7)−N(8)−Cu(1)	112.3(2)

The structural analysis of **1**, **2**, and **3** demonstrates the intrinsic property of the ligand H_4L to complex Cu^{2+}, Ni^{2+}, and Pd^{2+} in a 4-coordinate fashion, in spite of the varying ionic radii,[14] of Cu^{2+} 0.71 Å, Ni^{2+} 0.63 Å, and Pd^{2+} 0.78 Å. Such adaptability of a ligand to various metal ion sizes is not unknown.[15]

The molecular structure of complex **4** is shown in Figure 3. Selected bond distances and angles are listed in Table 3. The structure of the neutral 5-coordinated complex **4** contains the ligand in monoradical dianionic form, $[HL^{\bullet}]^{2-}$, whose presence is clearly established by single-crystal X-ray crystallography, discussed below.

The aromatic C−C bond distances for each individual unsubstituted phenyl ring in complex **4** have been found to lie within the small experimental error limits of 1.390 ± 0.01 Å, indicating that the biphenyl part of the ligand is redox innocent.

(11) (a) *ShelXTL*, v. 6.14; Bruker AXS Inc.: Madison, WI, 2003. (b) Sheldrick, G. M. *ShelXL97*; Universität Göttingen: Göttingen, Germany, 1997.

(12) Chaudhuri, P.; Verani, C. N.; Bill, E.; Bothe, E.; Weyhermüller, T.; Wieghardt, K. *J. Am. Chem. Soc.* **2001**, *123*, 2213.

(13) See for example: (a) Wehman, P.; Dol, G. C.; Moorman, E. R.; Kamer, P. C. J.; van Leeuwen, P. W. N. M.; Fraanje, J.; Goubitz, K. *Organometallics* **1994**, *13*, 4856. (b) Milani, B.; Anzilutti, A.; Vicentini, L.; O Santi, A. S.; Zangrando, E.; Geremia, S.; Mestroni, G. *Organometallics* **1997**, *16*, 5064. (c) Holm, R. H.; O'Connor, M. J. *Prog. Inorg. Chem.* **1971**, *14*, 241.

(14) Shannon, R. D. *Acta Crystallogr.* **1976**, *A32*, 751.

(15) Klein Gebbink, R. J. M.; Jonas, R. J.; Goldsmith, C. R.; Stack, T. D. P. *Inorg. Chem.* **2002**, *41*, 4633.

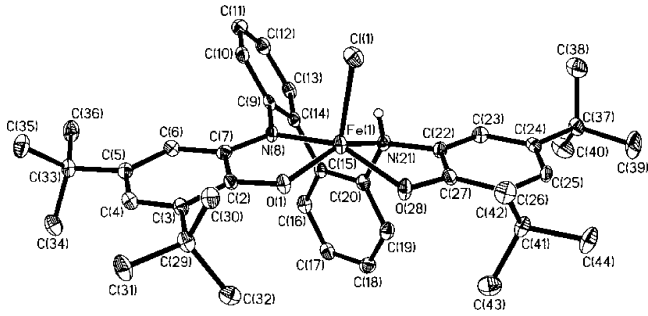

Figure 3. Oak Ridge Thermal Ellipsoid Plot (ORTEP) diagram of complex **4**, [Fe^{III}($HL^{\bullet}$)Cl], with 50% probability of the ellipsoids.

Table 3. Selected Bond Distances (Angstroms) and Angles (deg) for **4**, [Fe^{III}($HL^{\bullet}$)Cl]

Fe(1)−N(8)	2.044(2)	C(4)−C(5)	1.444(4)
Fe(1)−N(21)	2.206(3)	C(5)−C(6)	1.364(4)
Fe(1)−O(1)	1.943(2)	C(6)−C(7)	1.422(4)
Fe(1)−O(28)	1.905(2)	C(22)−N(21)	1.424(4)
Fe(1)−Cl(1)	2.228(1)		
C(2)−O(1)	1.305(3)	C(22)−C(23)	1.381(4)
C(7)−N(8)	1.345(4)	C(23)−C(24)	1.393(4)
C(2)−C(7)	1.453(4)	C(24)−C(25)	1.398(4)
C(2)−C(3)	1.426(4)	C(25)−C(26)	1.402(4)
C(3)−C(4)	1.371(4)	C(26)−C(27)	1.411(4)
C(9)−N(8)	1.424(4)	C(27)−O(28)	1.347(4)
C(9)−C(10)	1.389(4)	C(20)−C(15)	1.398(4)
C(10)−C(11)	1.383(4)	C(15)−C(16)	1.392(4)
C(11)−C(12)	1.384(4)	C(16)−C(17)	1.393(4)
C(12)−C(13)	1.382(4)	C(17)−C(18)	1.383(4)
C(13)−C(14)	1.396(4)	C(18)−C(19)	1.387(4)
C(14)−C(9)	1.409(4)	C(19)−C(20)	1.386(4)
O(1)−Fe(1)−N(8)	79.79(9)	O(1)−Fe(1)−O(28)	99.20(9)
N(8)−Fe(1)−N(21)	79.33(9)	O(1)−Fe(1)−N(21)	146.61(9)
N(21)−Fe(1)−O(28)	85.3(11)	O(28)−Fe(1)−N(8)	148.62(10)
C(27)−O(28)−Fe(1)	114.78(19)	C(2)−O(1)−Fe(1)	112.21(18)
C(22)−N(21)−C(20)	114.9(2)	C(7)−N(8)−C(9)	119.1(2)
Fe(1)−N(21)−C(20)	110.72(18)	C(9)−N(8)−Fe(1)	126.34(18)
C(22)−N(21)−Fe(1)	102.9(17)	C(7)−N(8)−Fe(1)	113.4(2)

The metal ion Fe(1) is 0.55 Å above the plane comprising N(8)O(1)O(26)N(21) atoms toward the apical Cl(1). The charge distributions in the ligand, acting, as expected, as a bis(O,N-bidentate) ligand, $(NO)_2$, with a biphenyl group as a spacer are different in the two sides, Fe(1)O(1)N(8) and Fe(1)N(21)O(28), of the iron-containing equatorial plane. The ligand-part containing the donor atoms O(1), N(8) exhibits typical characteristics of the charge distribution for o-iminobenzosemiquinonate(1-) π-radical,[7,12] short C(7)−N(8) and C(2)−O(1) bond distances at 1.345(4) and 1.305(3) Å, respectively, approaching double bonds together with the missing conjugation in the phenyl ring with C(2) to C(7) atoms containing the *tert*-butyl substituents: the typical pattern of the iminobenzosemiquinone radicals of a short, a long, and again a short, and three adjacent long C−C bonds are found, namely, C(3)−C(4) 1.371(4), C(4)−C(5) 1.444(4), C(5)−C(6) 1.364(4), C(6)−C(7) 1.422(4), C(7)−C(2) 1.453(4), C(2)−C(3) 1.426(4) Å. Thus, this phenyl ring adopts a quinoid-type structure. The coordination geometry around the nitrogen donor N(8) is planar, indicating that N(8) is three-coordinate (sp^2 hybridization) and not protonated. Thus, this part of the ligand displays the characteristic features of an O,N-coordinated iminosemiquinonate monoanion π-radical. The other part involving O(28)N(21) donor atoms acts as an aminophenolate monoanion with C(27)−O(28) 1.347(3) Å, C(22)−N(21) 1.452(4) Å and six equidistant C−C bonds at 1.397 (±0.016 Å) of the phenyl ring containing the *tert*-butyl substituents; the nitrogen atom N(21) is sp^3 hybridized with C(22)N(21)C(20) 114.9(2)°, C(20)N(21)Fe(1) 110.7(2)°, and C(22)N(21)Fe(1) 102.9(2)°, and thus bonded to a H atom, which has been detected also as a peak assignable to a proton in the later refinement stages; it was included in this position in the final refinement cycle. The presence of this single proton attached to N(21) renders this part of the ligand monoanionic. Thus, the ligand supplies two negative charges to the charge-balance consideration. The axial chloride ion Cl(1) completes the square-pyramidal geometry of the metal ion Fe(1). The Fe−O and Fe−N bond distances (Table 3) are consistent with a high-spin d^5 ferric ion description.

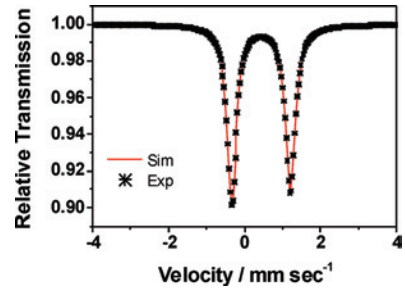

Figure 4. Zero-field Mössbauer spectrum of solid **4** at 80 K.

The zero-field Mössbauer spectrum (Figure 4) of solid complex **4** at 80 K corroborates the iron high-spin $3d(t_{2g})^3(e_g)^2$ configuration. The isomer shift $\delta = 0.44$ mm s^{-1} and quadrupole splitting $|\Delta E_Q| = 1.54$ mm s^{-1} are in accord with those reported[16] for square-pyramidal high-spin ferric species. The comparatively large quadrupole splitting for the 5-coordinate Fe(III) in **4** is not surprising, as in the high-spin iron(III) compounds with sextet spin multiplicity the quadrupole interaction does not provide a sensitive measure of the symmetry at the iron site. In summary, the crystal structure of **4** and its physical properties (loc. cit.) are in excellent agreement with a high-spin ferric(III)-formulation with one radical. Magnetic susceptibility measurements were performed on complex **4** (see later) to confirm this notion.

A perspective view of the metal (vanadium) coordination environment in **5** is shown in Figure 5. The metrical parameters for the two molecules in the unit cell are nearly identical and hence only one molecule is shown. The crystal structure reveals a divanadium complex, where the two vanadium atoms, V(1) and V(2), are in a similar six-coordination environment bridged by two methoxide oxygens. Each vanadium is terminally coordinated by two nitrogens and two phenolate oxygens of the 2,4-di-*tert*-butylphenol rings. Thus, each vanadium ion is in a N_2O_4 coordination environment. The equatorial plane of each vanadium ion consists of two methoxide oxygens, O(45) and

(16) (a) *Mössbauer Spectroscopy*; Dickson, D. P. E., Berry, F. J., Eds.; Cambridge University Press: Cambridge, 1986. (b) Chun, H.; Weyhermüller, T.; Bill, E.; Wieghardt, K. *Angew. Chem., Int. Ed.* **2001**, *40*, 2489. (c) Wyllie, G. R. A.; Murro, O. Q.; Schulz, C. E.; Scheidt, W. R. *Polyhedron* **2007**, *26*, 4664.

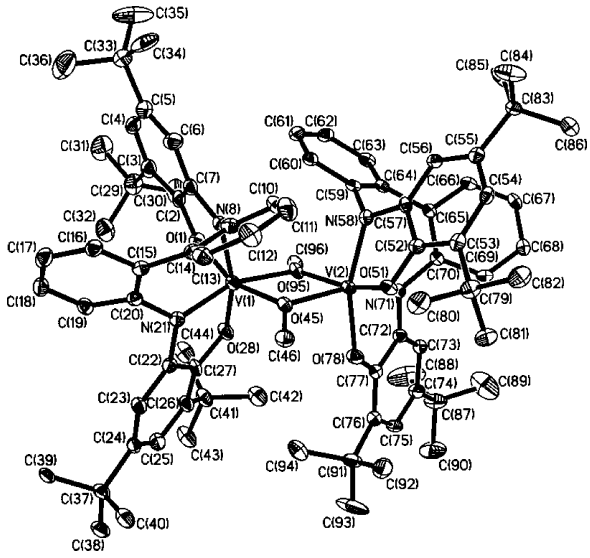

Figure 5. ORTEP diagram of complex **5**, $[L_2V_2(\mu\text{-}OCH_3)_2]$.

O(95), and one phenolate oxygen and one amido nitrogen, O(1), N(21) at V(1) and O(51), N(71) at V(2). The axial positions are occupied by a phenolate oxygen and an amido nitrogen, O(28), N(8) at V(1) and O(78), N(58) at V(2), respectively. Thus, the geometry around the two vanadium ions is distorted octahedral. The V(1)O(45)V(2)O(95) core is almost planar with the angle of 6° between the two planes comprising V(1)O(45)V(2) and V(1)O(95)V(2) atoms whereas V(1) is positioned out of the equatorial plane O(1)N(21)O(45)O(95) by 0.0274 Å, and V(2) is positioned more toward the plane O(51)N(71)O(45)O(95) with a deviation from the plane by 0.0168 Å. The nitrogens N(8), N(21), N(58), and N(71) are three-coordinate in a nearly planar geometry (sp^2-hybridization). The C−O and C−N distances related to the rings with the *tert*-butyl groups lie in the range 1.324(5)−1.334(5) and 1.372(5)−1.411(6) Å, respectively, indicating the corresponding bonds of order one, thus refuting the radical nature of the related phenyl rings. Notable also are the average C−C distances for the rings with and without *tert*-butyl groups at 1.400 ± 0.02 and 1.391 ± 0.017 Å, respectively, indicating clearly the aromatic nature of the rings and thus rendering the ligand to be an aromatic amidophenolate tetraanion. These X-ray results demonstrate clearly that compound **5** is correctly described with a physical oxidation state of +V for the vanadium ion. This conclusion corroborates the diamagnetic nature of the compound. Table 4 lists selected bond lengths and angles for complex **5**.

Magnetic Properties. Complexes **2**, **3**, and **5** possess an $S_t = 0$ ground-state as is clearly shown by the fact that the compounds display ^{1}H NMR spectra without detectable paramagnetic shifts or line broadening of the proton signals even at 298 K. Additionally, SQUID measurements show unambiguously their diamagnetic character. The ^{51}V NMR spectrum for complex **5** was also recorded to exhibit a broadband at $\delta \sim 120$ ppm with respect to $VOCl_3$. The downfield shift is presumably due to coordination of the central vanadium(v) ions with electron rich and strong π-donor amidophenolate and methoxide groups.

Table 4. Selected Bond Lengths (Angstroms) and Angles (deg) in **5**·1.25CH_2Cl_2

V(1)•••V(2)	3.120(1)		
V(1)−O(28)	1.884(3)		
V(1)−O(45)	1.908(3)		
V(1)−O(1)	1.919(3)		
V(1)−N(21)	1.950(3)		
V(1)−N(8)	1.958(4)		
V(1)−O(95)	2.057(3)		
V(2)−O(78)	1.894(3)		
V(2)−O(95)	1.904(3)		
V(2)−O(51)	1.916(3)		
V(2)−N(71)	1.962(3)		
V(2)−N(58)	1.964(4)		
V(2)−O(45)	2.049(3)		
O(1)−C(2)	1.326(5)		
O(28)−C(27)	1.331(5)		
O(51)−C(52)	1.324(5)		
O(78)−C(77)	1.334(5)		
N(8)−C(7)	1.373(6)		
N(21)−C(22)	1.406(5)		
N(58)−C(57)	1.372(5)		
N(71)−C(72)	1.411(6)		
O(28)−V(1)−O(45)	106.68(13)	V(1)−O(45)−V(2)	103.99(13)
O(28)−V(1)−O(1)	88.22(13)	V(1)−O(95)−V(2)	103.85(13)
O(45)V(1)−O(1)	159.10(13)		
O(28)−V(1)−N(21)	81.38(14)		
O(45)−V(1)−N(21)	96.96(13)		
O(1)−V(1)−N(21)	99.78(14)		
O(28)−V(1)−N(8)	162.75(15)		
O(45)−V(1)−N(8)	89.82(14)		
O(1)−V(1)−N(8)	77.26(14)		
N(21)−V(1)−N(8)	91.84(15)		
O(28)−V(1)−O(95)	82.24(12)		
O(45)−V(1)−O(95)	75.82(12)		
O(1)−V(1)−O(95)	92.23(12)		
N(21)−V(1)−O(95)	159.32(14)		
N(8)−V(1)−O(95)	107.29(13)		
O(78)−V(2)−O(95)	106.11(13)		
O(78)−V(2)−O(51)	89.69(13)		
O(95)−V(2)−O(51)	157.20(13)		
O(78)−V(2)−N(71)	81.29(13)		
O(95)−V(2)−N(71)	96.19(13)		
O(51)−V(2)−N(71)	102.50(14)		
O(78)−V(2)−N(58)	160.78(14)		
O(95)−V(2)−N(58)	90.49(13)		
O(51)−V(2)−N(58)	77.53(13)		
N(71)−V(2)−N(58)	87.46(14)		
O(78)−V(2)−O(45)	83.16(12)		
O(95)−V(2)−O(45)	76.08(12)		
O(51)−V(2)−O(45)	89.96(12)		
N(71)−V(2)−O(45)	159.95(14)		
N(58)−V(2)−O(45)	110.77(13)		

The magnetic properties of complexes **1** and **4** were probed by variable-temperature (2−290 K) magnetic susceptibility (SQUID) measurements and EPR spectroscopy. Complex **1**, a three-spin molecule with two radical ($S_R = {}^1/_2$) and one copper(II) ($S_{Cu} = {}^1/_2$) spins, possesses three coupled spin states, namely, $|S_t,S^*\rangle = |{}^1/_2,0\rangle$, $|{}^1/_2,1\rangle$, and $|{}^3/_2,1\rangle$ or pictorially (↑↑↓), (↑↓↑), and (↑↑↑), respectively, in which S_t represents the total spin $S_t = S_{Cu} + S_{R1} + S_{R2}$ and the subspin $S^* = S_{R1} + S_{R2}$. As an overall antiferromagnetic interaction in **1** is expected,[6d,12] the EPR spectrum of **1** was measured to determine which of the two doublets $|{}^1/_2,0\rangle$ or $|{}^1/_2,1\rangle$ constitutes the ground-state for complex **1**. This is possible because Cu(II) (d^9) ions exhibit significant g anisotropy and large hyperfine splitting contrasting in this respect to the

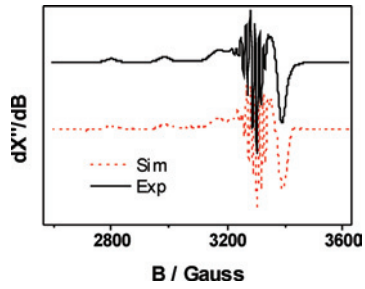

Figure 6. X-band EPR spectrum of **1** in CH_2Cl_2 at 10 K. Experimental parameters: frequency 9.48 GHz, power 10 μW, modulation 1 mT. The dotted line is a spin Hamiltonian simulation for total spin $S_t = {}^1/_2$ with parameters given in the text.

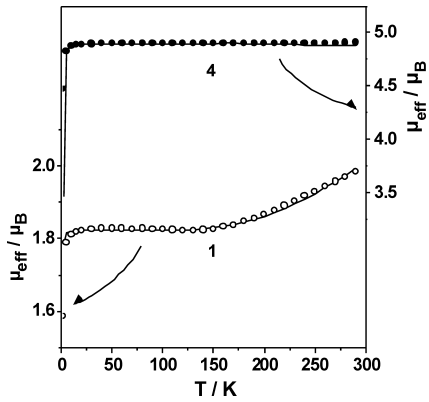

Figure 7. Simulated (solid lines) and experimental data for the μ_{eff} vs T plots of complexes **1** and **4**.

coordinated organic radical anions. The EPR spectrum of **1** in a CH_2Cl_2/toluene solution (1:1) at 10 K, shown in Figure 6, exhibits rhombic g values, $g_1 = 2.064$, $g_2 = 2.048$, $g_3 = 2.195$. Interestingly, the spectrum shows distinct ligand hyperfine splittings, barely resolved for the $g_{\|}$ lines but clearly so at g_x and g_y. A satisfactory simulation, shown also in Figure 6, was obtained with two equivalent ^{14}N nuclei ($I = 1$) with $A_N = (45, 40, \text{and } 20 \times 10^{-4}\ \text{cm}^{-1})$. The X-band EPR results indicate clearly that the ground spin state has predominantly metal(copper) character, with the spin-alignment ($\uparrow\uparrow\downarrow$), that is, the doublet state $|{}^1/_2,0\rangle$. Thus, it appears that the antiferromagnetic radical−radical interactions (J_R) dominate over the copper-radical interactions (J) in **1**, similar to that reported for other copper(II)-diradical complexes,[6d,12] and consequently, the exchange interactions lead to an almost "isolated" copper(II) spin character of the ground state.

That complex **1** has an $S_t = {}^1/_2$ spin ground-state is also evident from the thermal variation of the effective magnetic moments for **1**, shown in Figure 7. At temperatures 5−150 K, μ_{eff} remains virtually constant at 1.82 ± 0.01 μ_B. At temperatures above 150 K, μ_{eff} increases slowly reaching a value of $\mu_{eff} = 1.99\ \mu_B$ ($\chi_M T = 0.4917\ \text{cm}^3\ \text{mol}^{-1}\ \text{K}$) at 290 K, indicating population of the excited states. The 2J-model based on the Hamiltonian

$$\hat{H} = -2J(\hat{S}_{Cu}\cdot\hat{S}_{R1} + \hat{S}_{Cu}\cdot\hat{S}_{R2}) - 2J_R(\hat{S}_{R1}\cdot\hat{S}_{R2}) + g\mu_B\sum_i \hat{S}\cdot\vec{B} \quad (1)$$

was modified to $\hat{H} = -2J'_R\ (\hat{S}_{R1}\cdot\hat{S}_{R2}) + g\mu_B\sum_i\hat{S}\cdot\vec{B}$ for simulation, shown as the solid line in Figure 7. Simulation yields $J'_R = -357\ \text{cm}^{-1}$. In summary, we have simulated the magnetic data by keeping $J = 0$ (fixed), $g_R = 2.00$ (fixed) and $g_{Cu} = 2.104$ (fixed) as obtained from the EPR measurement. Thus, the single effective coupling constant, designated as $J'_R = -357\ \text{cm}^{-1}$, demonstrates the antiferromagnetic nature of the interaction between the radicals. An elaborate discussion on the constraint $|J_R| \gg |J|$ used for the simulation has been done in our earlier reports[6d,12] and hence we are refraining from discussing it again.

Thus, considering all the 4-coordinate copper(II)-diradical complexes reported till today[6d,12] together with complex **1**, it can be summarized that the antiferromagnetic radical−radical interactions ($J \approx$ ca. $-400\ \text{cm}^{-1}$) dominate over the copper-radical interactions, and the distortion of the copper coordination sphere from square planar because of the biphenyl moiety in **1** has no significant consequences on the magnetic exchange coupling.

Variable-temperature magnetic susceptibility measurements for **4** are shown in Figure 7 as a μ_{eff} vs T plot. The effective magnetic moments remain virtually constant at $\mu_{eff} = 4.85 \pm 0.10\ \mu_B$ in the temperature range 10−290 K, indicating a spin state $S_t = 2.0$ because of a strong antiferromagnetic spin coupling between h.s.Fe^{III} (d^5, $S_{Fe} = {}^5/_2$) and the radical anion ($S_R = {}^1/_2$). Additionally, thermal invariance of the magnetic moment in the range 10−290 K indicates that the upper-lying $S_t = 3.0$ state is positioned at more than 200 cm^{-1} higher in energy than the ground state $S_t = 2.0$.

Electro- and Spectroelectrochemistry and Electronic Spectra. Cyclic voltammograms (CV) of complexes **1**−**5** have been recorded in CH_2Cl_2 solutions containing 0.1 M $[N(n\text{-}Bu)_4]PF_6$ as the supporting electrolyte at a glassy carbon working electrode and a $Ag/AgNO_3$ reference electrode. Ferrocene was used as an internal standard and all potentials are referenced versus the ferrocene couple Fc^+/Fc.

The CVs of **1** (Cu) and **3** (Pd) are very similar and displayed in Figure 8. In both cases, four reversible one-electron transfer waves are observed of which, according to coulometric measurements, two correspond to reductions and two to oxidations. Since the redox potentials, summarized in Table 5, are similar irrespective of the nature of the central metal ion (copper or palladium) we assign these processes as ligand centered, as was also observed earlier for the analogous Cu(II)- and Pd(II)-diradical complexes.[6,12] These assignments are nicely corroborated by the electronic spectra of the electrochemically generated oxidized and reduced forms of **1** and **3**. Figure 9 displays these spectra of the copper complexes. The spectrum of the fully reduced form $[Cu^{II}(L^{AP}\text{-}4H)]^{2-}$ does not have any absorption above 400 nm. Upon one-electron reduction of [**1**] to [**1**]$^-$, the long-wavelength band at 882 nm of [**1**] attributable to intraligand and LMCT is shifted to 825 nm with reduced intensity for [**1**]$^-$. In contrast, a strong intervalence ligand-based band arises at ~1280 nm in addition to a sharp, strong band at 570 nm, possibly associated with the quinone-part of the ligand, for one-electron oxidized species [**1**]$^+$.

A notable feature in the UV−vis/NIR spectra for complexes **2** and **3** is very intense absorption band with a maximum in the range 700−1200 nm; 981 nm ($\varepsilon \sim 1.4 \times$

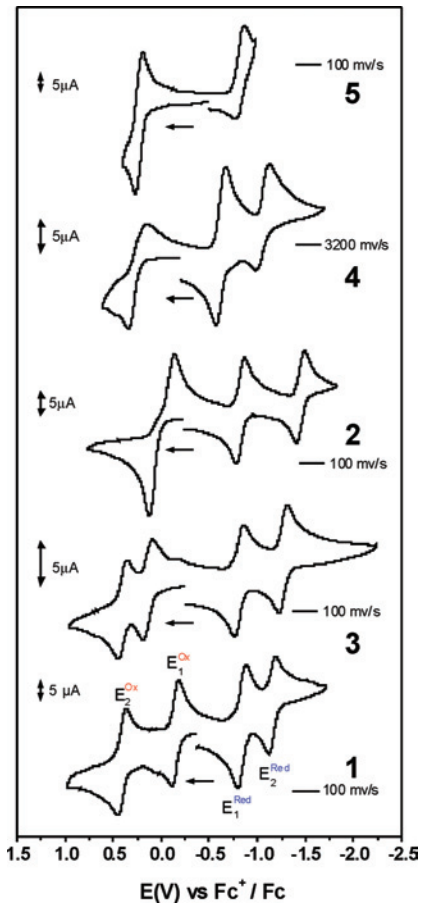

Figure 8. Cyclic voltammograms of complexes **1**−**5** recorded in CH_2Cl_2 solutions containing 0.1 M $[(n\text{-}Bu)_4N]PF_6$ as the supporting electrolyte at ambient temperatures and a scan rate of 100 mV s^{-1} except for **4**.

Table 5. Formal Electrode Potentials for Oxidation and Reduction (in V vs Fe^+/Fc) of Complexes **1**−**5**

complex	Ox2, V	Ox1, V	Red1, V	Red2, V
1 (Cu^{II})	+0.347	−0.16	−0.614	−0.984
2 (Ni^{II})	0.040[a]		−0.82	−1.45
3 (Pd^{II})	+0.39	+0.13	−0.80	−1.27
4 (Fe^{III})		+0.215	−0.615	−1.065
5 (V^{V})		+0.23	E(Peak) = −0.822	

[a] For 2e-process

10^4 M^{-1} cm^{-1}) for **2** and 961 nm ($\varepsilon \sim 2.7 \times 10^4$ M^{-1} cm^{-1}) for **3**. We assign them as before[12] to a spin- and dipole-allowed ligand-to-ligand transition. This intraligand charge transfer appears at a lower energy than that for the analogous previously reported complexes (~825 nm), presumably because of the tetrahedral distortion for **2** and **3** and thus differing from the structures of the analogous complexes described earlier.[12]

The CV of the quasi isostructural nickel(II)-diradical complex **2** is different from those of **1** and **3** in the anodic range (>0 V) and is depicted in Figure 8. The reduction of **2** is accomplished by two successive reversible one-electron-transfer waves at $E_{1/2}$ = −0.82 and −1.45 V which closely resemble those in **1** and **3** (Table 5). Therefore, we assign these reductions as ligand centered processes. Controlled-potential coulometric measurements established that the feature at E = 0.04 V (Figure 8) corresponds to one two-electron oxidation for **2**. Thus, for the oxidation process, there are two options: (i) direct oxidation of

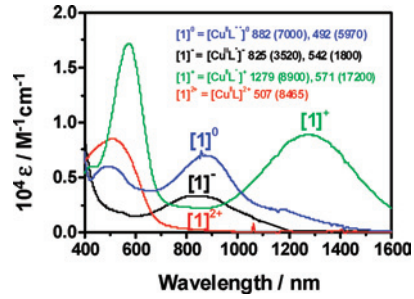

Figure 9. Electronic spectra of oxidized and reduced forms of **1** in CH_2Cl_2 solutions. The wavelengths (λ, nm) and extinction coefficients (ε, M^{-1} cm^{-1}) are denoted in the following way: $\lambda(\varepsilon)$.

the ligand from iminosemiquinone to iminoquinone form at the same potential, or (ii) the Ni(II) is oxidized to Ni(III) with subsequent intramolecular electron-transfer to the iminosemiquinone. As the oxidation potential is same for all the Ni(II)-diradical complexes (Table 5) reported in the literature,[8,12] the mechanism for the oxidation process can safely be assumed to be the same as has been described by us earlier; hence, we are refraining from discussing the mechanism again in detail.

The electronic spectrum of **4** in CH_2Cl_2 exhibits two very intense bands of nearly equal intensity at 443 and 710 nm ($\varepsilon = 1.1 \times 10^{-4}$ M^{-1} cm^{-1}), which are assigned to LM and intraligand intervalence charge transfer, respectively. Complex **4** shows a one-electron quasi-reversible wave at +0.215 V (oxidation) and two reversible one-electron-transfer waves at −0.615 V and −1.065 V (reduction), as judged by the controlled potential coulometric measurements. Upon one-electron reduction, a broadband at ~530 nm ($\varepsilon \sim 6700$ M^{-1} cm^{-1}) for $[\mathbf{4}]^-$ appears and is assignable to phenolate-to-iron charge transfer. A CV of **4**, using a Pt working electrode at a fast scan rate, is shown in Figure 8.

Within the potential range −1.2 V to +0.7 V, one reversible oxidation at +0.23 V and one irreversible reduction, $E_{pa} \sim$ −0.822 V processes are observed for complex **5**.

Catalytic Oxidation of Benzylalcohol. We have examined the catalytic activity of complex **1** for the oxidation of benzyl alcohol by air to benzaldehyde in dichloromethane according to the reaction

$$C_6H_5CH_2OH + O_2 \xrightarrow[CH_2Cl_2]{\text{complex}\mathbf{1},\ \text{Air}} C_6H_5CHO + H_2O_2 \quad (2)$$

The reactivity studies were performed in dichloromethane because of the good solubility of the complex as well as of the substrate and of its product.

The catalytic process is strongly base-dependent. Prior to a detailed kinetic study, we quantitatively evaluated the base dependence, which is depicted in Figure 10 as a plot of yield of benzaldehyde (%) versus the concentration of Bu_4NOMe. The concentration of PhCHO was determined by LC. A weak base like triethylamine results in a low turnover number (TON) of only 7/15 h. Alternatively, a stronger base, $^nBu_4NOMe$, yields a higher TON for the catalytic oxidation. By varying the concentration of $^nBu_4NOMe$, the conversion percentage can be improved and a maximum yield is obtained when the concentration of the base is 90% of the total concentration of the substrate benzyl alcohol (Figure 10).

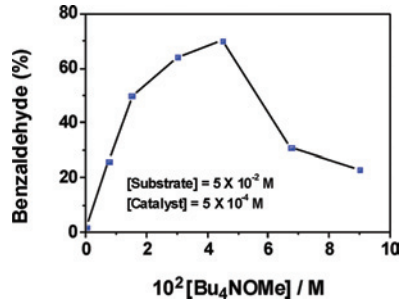

Figure 10. Effect of [Base] on the percentage of oxidized benzylalcohol.

Further increase in the concentration of the base inhibits the catalysis, presumably because of the coordination of excess base (methoxide) to the copper(II) center of **1**, thus hindering benzyl alcoholate anion from coordination. It is noteworthy that complex **1** is incapable of oxidizing methoxide to formaldehyde, as reported earlier by us for a copper(II)-diradical complex.[6d]

Reaction kinetics were performed by observing the change in absorbance at 290 nm ($\varepsilon \sim 1220$ M^{-1} cm^{-1}), which is characteristic of benzaldehyde, using the catalyst solution as a blank. We have measured the kinetics of the oxidative catalysis at 22 ± 1 °C using the initial rate method, where the concentration of the catalyst was varied in the range of 2.5×10^{-4} M to 10×10^{-4} M and that of benzyl alcohol was in the range of 5×10^{-4} to 5×10^{-2} M. From variation of the velocity as a function of substrate concentration, the rate of the reaction with respect to substrate was found to be first order with $k_{sub} = 2.3$ min^{-1}. Similar procedures with varying catalyst concentrations keeping a constant substrate concentration (5×10^{-2} M) yielded different velocities, thus leading to the result for the order of the reaction with respect to the catalyst. A first-order dependence with $k_{cat} = 2.2 \times 10^2$ min^{-1} was obtained, resulting in an overall rate-law

$$\text{Rate} = k[\text{complex}][\text{PhCH}_2\text{OH}]$$

The observed first order dependence on both the catalyst and substrate concentrations implies that the four-coordinated Cu(II) center in **1** binds a substrate alcohol molecule with formation of a five coordinate intermediate (see mechanistic scheme); in other words, the composition of the activated complex consists of one molecule of complex **1** and one molecule of alcohol for the two-electron oxidation process. Turnover numbers (TON) as a function of benzylalcohol concentration with [complex **1**] = 5×10^{-4} M, shown in Figure 11b, exhibit saturation kinetics implying a comparatively high binding constant for the substrate.

To shed more light on a qualitative mechanism of this two-electron oxidation process, we performed additional experiments to point out the followings: (i) H-atom abstraction is probably involved in the rate-determining step; (ii) oxygen of air is essential for the catalysis; (iii) the radicals coordinated to the copper(II) center in **1** are participating in the redox process; and (iv) the fate of oxygen (air) involved.

The kinetics of the oxidation of benzylalcoholate to benzaldehyde using the deuterated substrate $PhCD_2OH$ have been measured and the change in the concentration of benzaldehyde with time is shown for both $PhCH_2O^-$ and

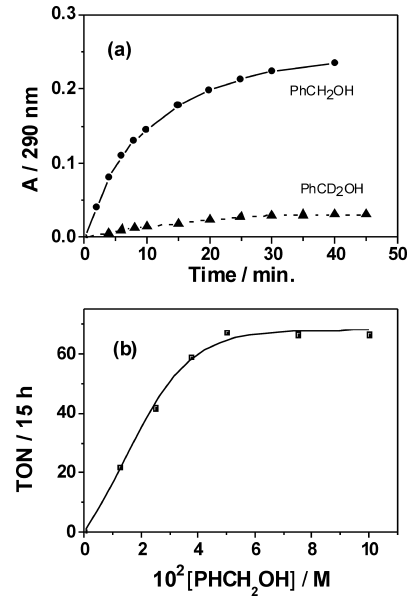

Figure 11. (a) Plots of change in absorption (i.e., [Benzaldehyde]) with time to evaluate the primary KIE. (b) Turnover numbers (TON) as a function of benzylalcohol concentration for the aerial oxidation of benzylalcohol catalyzed by **1** (5×10^{-4} M) in CH_2Cl_2.

$PhCD_2O^-$-substrates in Figure 11a. The k_H/k_D ratio of ~14 indicates remarkable primary kinetic isotope effect (KIE) and suggests H-atom abstraction from the α-carbon atom of the coordinated alcoholate to be the rate-determining step. The resulting ketyl radical, known to be a strong one-electron reductant, is converted to aldehyde via an intramolecular electron-transfer step (see the mechanistic scheme). As for copper, a late transition element, the other two possibilities (i) SET/proton transfer and (ii) hydride transfer, are also important; we consider KIE of ~14 only as a strong indication for the H-atom transfer.

Reaction under Anaerobic Conditions in a Glovebox. One equivalent of complex **1**, 10 equiv of the substrate $PhCH_2OH$, and 9 equiv of $^nBu_4NOMe$ in CH_2Cl_2 were allowed to react for 20 h under argon in a glovebox.

An aliquot of this reaction solution was divided into several parts to (i) determine strictly under argon the amount of benzaldehyde formed in absence of air, (ii) record UV−vis/NIR spectrum of the reaction solution strictly under argon, and (iii) measure the concentration of hydrogen peroxide after aerial extraction into an aqueous phase from the reaction solution by the titanyl(IV) sulfate reagent.

From the quantitative LC study, interestingly the formation of only 0.5 equiv of benzaldehyde could be observed indicating that only one electron of the catalyst (**1**) is involved. This is also substantiated by comparing the optical spectra of the reaction solution in the glovebox with that of the species $[Cu^{II}L^{\bullet}]^{1-}$, $[\mathbf{1}]^-$, obtained from one-electron electrochemical reduction of complex **1** (Figure 9); they exactly match with each other. The anaerobic reaction is thus an indication that the mechanism of this oxidation reaction is unlike that of Galactose Oxidase.[1]

Although the presence of hydrogen peroxide in the catalytic solution could be detected spectrophotometrically ($\lambda = 408$ nm, $\varepsilon \sim 675$ M^{-1} cm^{-1}) with certainty through

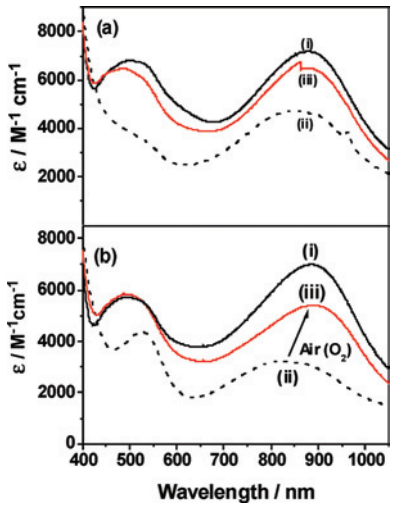

Figure 12. (a) Change in electronic spectra during and after the catalysis: (i) complex **1** before addition of benzylalcohol and [*n*-Bu_4]NOMe; (ii) during the catalysis in the presence of air; (iii) after 16 h of the catalytic reaction. (b) Effect of base on the electronic spectra of catalyst, complex **1**: (i) complex **1** under argon; (ii) complex **1** on addition of base under argon; (iii) after exposure of solution ii to air. The electronic spectrum changes from (i) → (ii) → (iii).

the formation of yellow titanyl peroxide, the concentration determination could not be performed very accurately presumably because of decomposition at a fast rate of the formed H_2O_2 in the prevailing strongly basic medium. The extremely slow nature of the oxidation prevented us also from examining the O_2-uptake measurements accurately.

The optical absorption spectral measurements (Figure 12a) during the catalytic reaction show the presence of $[Cu^{II}(L^{\bullet})]^-$, which is oxidized back to the neutral biradical complex $[Cu^{II}(L^{\bullet\bullet})]$ after the catalytic reaction by air. The experimental fact depicted in Figure 12 leads to the notion that the neutral complex **1**, $[Cu^{II}(L^{\bullet\bullet})]$, is not the active species but some other species is catalytically active.

The catalytic process is strongly base-dependent as stated earlier (Figure 10); hence, the effect of the base on the absorption spectra of **1** has been investigated in detail. Figure 12b shows the change of optical spectrum of **1** upon addition of the base $^nBu_4$NOMe under argon, indicating the decrease in absorption as an effect of the base. The decrease in absorption can be attributed to the disproportionation reaction shown below

$$2[Cu^{II}(L^{\bullet})]^0 \xrightarrow{\text{Base}} [Cu^{II}(L^{\bullet})]^+ + [Cu^{II}(L^{\bullet})]^- \qquad (3)$$

To substantiate this disproportionation reaction in the base, the absorption spectra of three different solutions of complex **1** (4.75×10^{-4} to 1.27×10^{-3} M) containing different amount of the base (2.8×10^{-3} to 7.5×10^{-3} M) were measured keeping the ratio [Base]/[Complex] = 6 for each solution. The absorption values observed, for example, at 880 nm have been found to be equal to the sum of the absorptions for $[Cu^{II}(L^{\bullet})]^+$ and $[Cu^{II}(L^{\bullet})]^-$, 50% each relative to the total concentration of $[Cu^{II}(L^{\bullet\bullet})]^\circ$. The extinction coefficients for each species were obtained from the spectroelectrochemical measurements (Figure 9). Though the mechanism of the disproportionation reaction is yet to be resolved, the matching of the absorption values supports the disproportionation nature of the reaction as the effect of the base on the catalyst in solution. A weak base like Et_3N cannot cause any change in the optical spectra.

As the monoradical monoanionic species $[Cu^{II}(L^{\bullet})]^-$ is observed during the aerial catalytic reaction (Figure 12a), it is conceivable that the neutral diradical complex **1**, $[Cu^{II}(L^{\bullet\bullet})]^\circ$, disproportionates to the monoanionic species $[Cu^{II}(L^{\bullet})]^-$ and the monocationic species $[Cu^{II}(L^{\bullet})]^+$ in the presence of a strong base like $^nBu_4$NOMe thus rendering the monocationic form $[Cu^{II}(L^{\bullet})]^+$ catalytically active; hence, the catalytic solution, that is, in the presence of the substrate, exhibits optically only the existent monoanionic form $[Cu^{II}(L^{\bullet})]^-$. The invisibility of 50% catalytic species, $[\mathbf{1}]^+ + PhCH_2O^-$, might indicate involvement of Cu(I)-species during the electron-transfer process, which is not included in Scheme 2.

On the basis of the kinetic and electrochemical data together with the anaerobic experiments described earlier, it is tempting to propose a mechanism involving stepwise pathways, keeping in mind that we do not want to draw any definitive conclusion. A speculative but very likely catalytic cycle for the oxidation of benzyl alcohol is shown in Scheme 2, without considering the possibility of the Cu(I)-species formed during the catalytic process.

Concluding Remarks and Outlook. We report a new redox-active ligand incorporating N_2O_2 donor atoms, which can yield metal-radical complexes. Crystallographic bond parameters, spectral and magnetic properties were collectively used to determine the electronic structures of the complexes synthesized; the new ligand with a biphenyl backbone can induce, as expected, a tetrahedral distortion of the metal(II) geometry having a N_2O_2 coordination environment. Strong antiferromagnetic exchange interactions have been established from the variable-temperature magnetic susceptibility measurements (2−290 K) between the radical centers. An apparent one-*J* model has been applied to establish the dominance of radical−radical interactions over the metal-radical interactions.

Electrochemical measurements indicate redox processes that are predominantly ligand centered. Thus, for complexes **1** (Cu^{II}), **2** (Ni^{II}), and **3** (Pd^{II}), two oxidations resulting in the quinone forms and two reductions resulting in the amidophenolate forms of the ligand are discernible.

The copper(II) complex, **1**, opened up an interesting opportunity of mimicking the functional property of the copper-enzyme, Galactose Oxidase, by investigating catalytically the oxidation of benzyl alcohol with aerial oxygen. From the perspective of the recent emergence of amino acid radical enzymology, we successfully combined the merits of a new redox-active ligand and different metal ions to synthesize metal-radical complexes and investigated oxidases-like reactivity of complex **1**. A ligand-derived redox activity with a disproportionation reaction of the catalyst, **1**, has been proposed for the catalytic process, in which hydrogen-atom abstraction, as evidenced by the presence of KIE ($k_H/k_D \sim 14$), is the rate-determining step. The catalytic mechanism distinguishes itself from that of Galactose Oxi-

Scheme 2. Likely Mechanism for the Aerial Oxidation of Benzylalcohol Catalyzed by Complex **1**

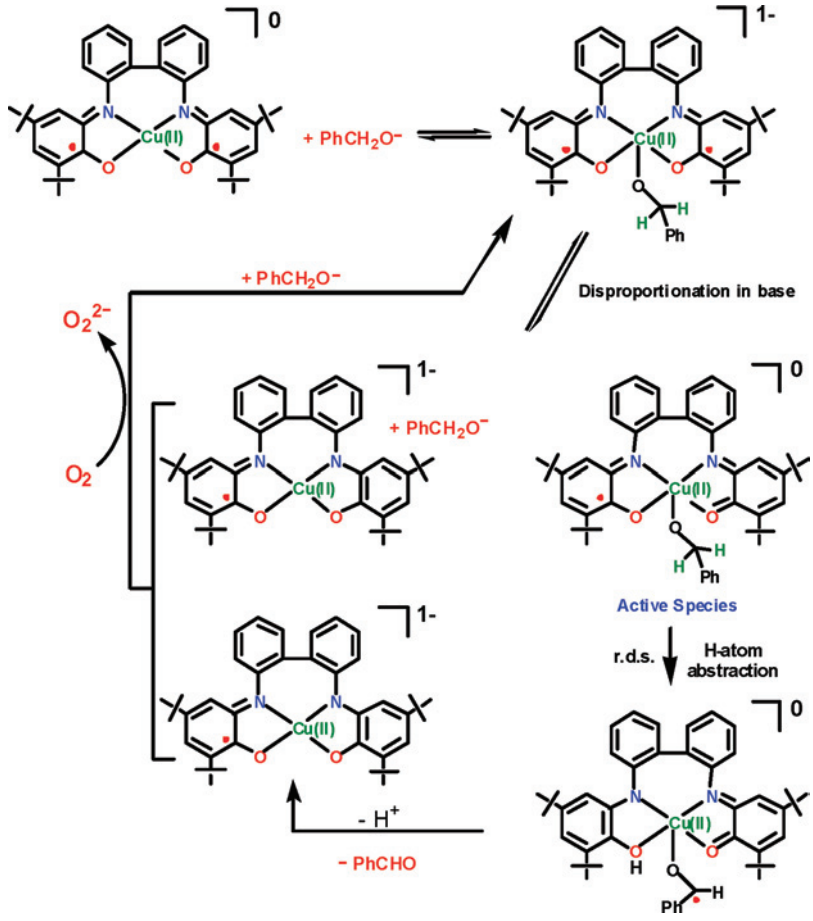

dase in that the redox activity of the catalysis derived primarily from the ligand without apparent participation of the copper center.

At the very outset no interesting chemistry has emerged from this new redoxactive tetradentate ligand H_4L with N_2O_2 donor atoms with respect to that reported earlier by us with the bidentate NO donor ligand H_2L_1 (Scheme 1); the ligand H_4L can be conceived as a simple dimer of H_2L_1. Specifically, the tetrahedral distortion of the coordination geometry has led neither to a different spin exchange mechanism nor resulted in a more effective catalyst than that with the ligand H_2L_1. To conclude, it is appropiate to mention here a few noteworthy aspects of the present ligand H_4L. (i) In contrast to H_2L_1, H_4L can provide not only biradical but also monoradical homoleptic complexes. (ii) Disproportionation of the copper(II) complex, **1**, implied in the mechanism of catalysis, is noteworthy. Such a disproportionation reaction has not been observed for the copper(II) complex $[Cu^{II}(L_1^{\bullet})_2]$,[6d] described earlier for the catalytic oxidation of primary alcohols. (iii) The present ligand is unique because of its unambiguous hydrogen atom abstraction. The KIE shown by complex **1** is remarkably high in comparison to that for the corresponding copper (II) complex with the ligand H_2L_1, that is, $[Cu^{II}(L_1^{\bullet})_2]$. (iv) H_4L can induce a tetrahedral distortion of the coordination geometry. Moreover, according to the Pauling electronegativies,[17] Cu, Ni, and Pd are relatively electronegative, that is, reluctant to release electrons, resulting in making them weak π-donors. Hence, the ligand $[L^{\bullet\bullet}]^{2-}$ in **1**, **2**, and **3** is subjected to attack by nucleophiles, thus opening the possibilities for application of **1**, **2**, and **3** in organic synthesis. In essence, the present study provides a lot of insights into the properties of metal-radical species that play important roles in governing reactivities of metalloenzymes and thus suggests a future direction for producing new bioinspired catalysts based on these metal-radical motifs.

Acknowledgment. Financial support from the Max-Planck Society and German Research Council (Deutsche Forschungsgemeinschaft) is gratefully acknowledged (Priority Program "Radicals in Enzymatic Catalysis" Ch 111/2-3). Skilful technical assistance of U. Pieper is thankfully acknowledged.

Supporting Information Available: Perspective views of **2** and **3**; selected bond lengths and angles for H_4L, **2,** and **3** (Tables S1−S3). This material is available free of charge via the Internet at http://pubs.acs.org.

IC8011734

(17) Pauling, L. *The Nature of the Chemical Bond*; Cornell University: Ithaca, NY, 1960.